Atmos. Meas. Tech. Discuss., 6, 5195–5216, 2013
www.atmos-meas-tech-discuss.net/6/5195/2013/
doi:10.5194/amtd-6-5195-2013

Atmospheric Measurement Techniques Discussions
Open Access

Characterization of the planetary boundary layer height and structure by Raman lidar: comparison of different approaches

D. Summa[1], P. Di Girolamo[1], D. Stelitano[1], and M. Cacciani[2]

[1]Scuola di Ingegneria, Università degli Studi della Basilicata, Viale dell'Ateneo Lucano n. 10, 85100 Potenza, Italy
[2]Dipartimento di Fisica, Università degli Studi di Roma "La Sapienza", Piazzale Aldo Moro, 2, 00100 Roma, Italy

Received: 14 May 2013 – Accepted: 23 May 2013 – Published: 13 June 2013

Correspondence to: D. Summa (donato.summa@unibas.it)

Published by Copernicus Publications on behalf of the European Geosciences Union.

Abstract

The Planetary Boundary Layer (PBL) includes the portion of the atmosphere which is directly influenced by the presence of the Earth's surface. Aerosol particles trapped within the PBL can be used as tracers to study the boundary-layer vertical structure and time variability. As a result of this, elastic backscatter signals collected by lidar systems can be used to determine the height and the internal structure of the PBL.

The present analysis considers three different methods to estimate the PBL height. A first method is based on the determination of the first order derivative of the logarithm of the range-corrected elastic lidar signals. Estimates of the PBL height for specific case studies obtained from this approach are compared with simultaneous estimates from the potential temperature profiles measured by radiosondes launched simultaneously to lidar operation. Additional estimates of the boundary layer height are based on the determination of the first order derivative of the range-corrected rotational Raman lidar signals. This latter approach results to be successfully applicable also in the afternoon-evening decaying phase of the PBL, when the effectiveness of the approach based on the elastic lidar signals may be compromised or altered by the presence of the residual layer. Results from these different approaches are compared and discussed in the paper, with a specific focus on selected case studies collected by the University of Basilicata Raman lidar system BASIL during the Convective and Orographically-induced Precipitation Study (COPS).

1 Introduction

The planetary boundary layer (PBL) is the lower region of the atmosphere directly in contact with the Earth's surface and strongly influenced by this surface. In this layer physical quantities such as flow velocity, temperature and moisture display rapid fluctuations associated with turbulent motion and vertical mixing.

AMTD
6, 5195–5216, 2013

The characterization of the planetary boundary layer is of primary importance in a variety of fields as weather forecasting, climate change modelling and air quality prediction (Melfi et al., 1985; Flamant et al., 1997). The structure of the PBL can be complex and highly variable (Stull, 1988; Garratt, 1992). The PBL height is commonly used to characterize the vertical extent of mixing within the boundary layer and the height at which exchange with the free troposphere takes place (among others, Seibert et al., 2000).

Aerosol particles trapped within the PBL can be used as tracers to study the boundary-layer vertical structure and time variability. In fact, aerosols uplifted after sunrise by convective mixing can act as efficient tracers of the atmospheric portion over which the mixing occurs (among others, Flamant et al., 1997). Aerosols can also be dispersed out of the PBL during strong convective events or temporary breaks of the capping temperature inversion. Thus, elastic backscattered signals from aerosol particles measured by lidar systems can be used to determine the height and internal structure of the PBL and, when possible, of the residual layer (Melfi et al., 1985; Di Girolamo et al., 1999).

Several methods have been applied to estimate the PBL height and structure and their variability from the elastic lidar signals in the presence of mixed, stable and residual boundary layers (Melfi et al., 1985; Hooper and Eloranta, 1986; Boers et al., 1988; Flamant et al., 1997; Hayden et al., 1997; Di Girolamo et al., 1999; Seibert et al., 2000; Sicard et al., 2006). However, the complexity of the phenomena occurring within the PBL and the influence of advection and local accumulation processes in many cases prevent an unambiguous determination of the PBL height from elastic lidar signals, especially when aerosol stratifications are present within the PBL (Haeffelin et al., 2012).

An alternative lidar approach applicable is based on the application of a Haar wavelet covariance transform to lidar backscatter profiles to provide automated detection of the boundary layer top from by locating the maximum in the covariance profiles (Mallat and Hwang, 1992; Brooks, 2003; Morille et al. 2007).

AMTD
6, 5195–5216, 2013

A convenient, reliable and widely used approach for the determination of the boundary layer height and structure both in daytime and nighttime is represented by the identification of local maxima in the potential temperature vertical gradient profiles as measured by radiosondes (Cramer, 1972; Oke, 1988; Stull, 1988; Sorbjan, 1989; Garratt, 1992; Van Pul et al., 1994; De Wekker et al., 1997; Martucci et al., 2007). In fact, potential temperature tends to keep nearly constant with height within the mixed layer. The level of the maximum vertical gradient in potential temperature indicates the transition from a convectively unstable region, located below this maximum, to a stable or more stable region, located above the maximum. At the top of the mixed layer a stable layer is frequently present to stop the turbulent eddies from further rising. Very stable layers characterized by increasing temperature with height (called capping inversions) can keep deep convection from developing.

During the day, the level at which air parcels become negatively buoyant corresponds to a main temperature inversion. Convection is often observed to erode this inversion, permitting the buoyant air parcel to lift further up. When turbulence weakens in the afternoon, the temperature inversion builds up again, and this translates into a narrowing of the mixing region.

However, a fraction of aerosols can remain aloft, with limited subsidence. In these cases, the strong aerosol gradient observed in the afternoons and after-sunset is representative of a residual aerosol layer aloft the actual mixed layer. In these cases, the application of the PBL height estimate approach based on the use of the first order derivative of the logarithm of the range corrected elastic signals usually fails. Same is true for the approach based on the application of a Haar wavelet covariance transform to lidar backscatter profiles, as in fact after daytime convection ceases, aerosol layers may become stratified and multiple layers can form near the surface, thus preventing this algorithm to distinguish the top of the boundary layer and the top of the residual layer. In this situation alternative estimates of the PBL height can still be obtained from the rotational Raman lidar signals used for temperature measurements as proposed here. This approach is introduced and tested for the first time in the present paper. As

AMTD
6, 5195–5216, 2013

the residual layer height corresponds to a higher altitude temperature inversion (Martucci et al., 2010), the rotational Raman signals can potentially be used to infer both the mixed layer and the residual layer height.

Based on the above considerations, in the present work three different approaches to characterize the PBL height and structure are compared. A first approach is based on the application of the first order derivative to the logarithm of the range-corrected elastic signals (in what follows specified as "approach(1)"). A second approach considers the application of the same algorithm to the low-quantum number rotational Raman lidar signals which are typically used for temperature measurements (in what follows specified as "approach(2)" or rotational Raman approach). Signals used to test these two approaches are provided by BASIL, which is a Raman lidar system with temperature measurement capability. Results from these two approaches are compared with simultaneous estimates from the traditional approach which considers local maxima in the potential temperature vertical gradient profiles measured by radiosondes. The analysis is applied to eight selected case studies from the COPS experiment, which are characterized by different meteorological conditions.

The outline of the paper is the following: Sect. 2 provides a short description of the Raman lidar system BASIL, together with brief information on the COPS experiment and its observation strategy. In Sect. 3 a description of the different approaches is given and the results are illustrated and compared. Finally, in Sect. 4 all results are summarized.

2 BASIL

The University of BASILicata Raman Lidar system (BASIL) was deployed in Achern (Black Forest, Germany, Lat: 48.64° N, Long: 8.06° E, Elev.: 140 m) in the frame of the Convective and Orographically-induced Precipitation Study – COPS (Wulfmeyer et al., 2008, 2011). The COPS experiment was held in Southern Germany and Eastern France in the period 1 June–31 August 2007, as part of the German Research

AMTD
6, 5195–5216, 2013

Foundation (DFG) Priority Program 1167 "Quantitative Precipitation Forecast", with the overarching goal of advancing the quality of forecasts of orographically induced convective precipitation by four-dimensional observations and modelling of its life cycle (Kottmeier et al., 2008; Kalthoff et al., 2009; Wulfmeyer et al., 2011). During COPS, BASIL operated between 25 May and 30 August 2007 and collected more than 500 h of measurements, distributed over 58 measurement days and 34 intensive observation periods (IOPs). Quick-looks of these dataset are available on the COPS Website (http://www.cops2007.de/), under Operational Products, while water vapour and particle backscatter data for the most important IOPs can be downloaded from the World Data Center for Climate (http://cera-www.dkrz.de/WDCC/ui/BrowseExperiments.jsp?proj=COPS). All other data from BASIL can be directly requested to the authors of this paper.

The major feature of BASIL is represented by its capability to perform high-resolution and accurate measurements of atmospheric temperature and water vapour, both in daytime and night-time, based on the application of the rotational and vibrational Raman lidar techniques in the UV (Di Girolamo et al., 2004, 2006, 2009a; Bhawar et al., 2011). Besides temperature and water vapour, BASIL provides measurements of the particle backscattering coefficient at 355, 532 and 1064 nm, of the particle extinction coefficient at 355 and 532 nm and of particle depolarization at 355 and 532 nm (Griaznov et al., 2007; Di Girolamo et al., 2009b, 2012a, b; Maestri et al., 2010). A block diagram of the considered system is illustrated in Fig. 1. COPS measurement strategy consider a transect of five Supersites from the Vosges Mountains to the lee side of the Black Forest, crossing the Rhine valley, the Hornisgrinde Mountain and the Murg Valley. During COPS BASIL was located in the Rhine Valley Supersite (Supersite R). A variety of sensors were present in all Supersites: soil moisture sensors, turbulence or energy balance stations, radiosonde launching facilities, GPS tomography, and surface meteorological stations; most supersites were also equipped with lidars, radars and microwave radiometers. The variety of remote-sensing systems at each supersite

AMTD
6, 5195–5216, 2013

and the potential synergystic use of those is a peculiar aspect of the COPS experiment (Wulfmeyer et al., 2008).

3 Results

The algorithm which is considered in this work to estimate the PBL height from the Raman lidar data considers the quantity:

$$D(z) = \frac{\mathrm{d}}{\mathrm{d}z}(\ln[P_\lambda(z)z^2]) \quad (1)$$

where $P_\lambda(z)$ is either the elastic lidar signal at 1064 nm, $P_{\lambda_{\mathrm{El}}}(z)$, (considered in approach(1)) or the low-quantum number rotational Raman lidar signal, $P_{\lambda_{\mathrm{LoJ}}}(z)$, (considered in approach(2)) and the quantity $P_\lambda(z)\,z^2$ represents the range correct lidar signal. In the application of expression (1), different integration times are considered for $P_{\lambda_{\mathrm{El}}}(z)$ and $P_{\lambda_{\mathrm{LoJ}}}(z)$. Specifically, an intergration time of 10 min is considered for $P_{\lambda_{\mathrm{El}}}(z)$, while an intergartion time of 30 min is considered for $P_{\lambda_{\mathrm{LoJ}}}(z)$, this latter being characterized by smaller signal-to-noise ratios.

The minima of the quantity $D(z)$ identify the transitions between different layers. Thus the largest minimum usually identifies the boundary layer height. This approach is identified hereafter as "approach(1)" when applied to elastic lidar signals at 1064 nm, while it is identified as "approach(2)" or rotational Raman approach when applied to the low-quantum number rotational Raman lidar signals. For the purpose of this study, "approach(1)" was applied to the elastic lidar signals at 1064 nm and not to the elastic lidar signals at 532 and 355 nm, because of the larger sensitivity of the elastic lidar signals at 1064 nm to aerosols and their variability.

Potential temperature profiles, $T_{\mathrm{pot}}(z)$, obtained from the radiosonde data were also used to get additional estimates of the boundary layer height. This approach considers the maximum in the derivative of $T_{\mathrm{pot}}(z)$, which identifies the height of maximum gradient.

AMTD
6, 5195–5216, 2013

As already emphasized earlier, approach(2) is introduced and tested for the first time in the present paper. In this respect, we need to recall that temperature measurements are performed by BASIL through the application of the rotational Raman lidar technique in the UV, which is based on the detection of pure rotational Raman scattering from oxygen and nitrogen molecules. These rotational lines fall within two narrow spectral bands in the proximity of the laser wavelength, one including rotational lines characterized by low quantum rotational numbers, $P_{\lambda_{LoJ}}(z)$, and the other including rotational lines characterized by high quantum rotational numbers, $P_{\lambda_{HiJ}}(z)$. Atmospheric temperature measurements can be obtained from the power ratio of high-to-low quantum number rotational Raman lidar signals. Both $P_{\lambda_{LoJ}}(z)$ and $P_{\lambda_{HiJ}}(z)$ are characterized by a strong sensitivity to temperature variations, the sensitivity being anyhow slightly larger for the signal $P_{\lambda_{LoJ}}(z)$ than for $P_{\lambda_{HiJ}}(z)$. Additionally, $P_{\lambda_{LoJ}}(z)$ is characterized by a smaller random uncertainty, as a result of the smaller bandwidth of the interference filter used for the selection of this signal. Thus, in approach(2) of the present paper, expression (1) is applied to the rotational Raman signal $P_{\lambda_{LoJ}}(z)$.

Figure 2 shows the variability of the different quantities considered in the three approaches. Specifically, Fig. 2a illustrates the 10 min average profile of $P_{\lambda_{El}}(z)$ centered at 17:04 UTC on 30 July, which reveals the presence of a strong gradient around 3000 m, this corresponding to the temperature inversion simultaneously observed by the radisonde (launched at 17:04 UTC) and by the lidar system (Fig. 2b). Figure 2c illustrates the vertical gradient of $P_{\lambda_{El}}$ for the same 10-min time interval considered in Fig. 2a, while Fig. 2d illustrates the vertical gradient of $P_{\lambda_{LoJ}}(z)$ for this same time interval. The vertical gradient profiles in Fig. 2c–d reveal the presence of the subsequent minima which are used to identify the PBL height.

We preliminary tested these approaches on three selected case studies (15, 25 and 30 July 2007), but we then extended the analysis to additional case studies (eight in total) covering a variety of boundary layer conditions (see Table 1). Figure 3a illustrates the time evolution of the particle backscattering ratio at 1064 nm, $R_{1064}(z)$, on 15 July 2007 covering the time interval from 04:50 to 20:30 UT. Figure 3b illustrates the

AMTD
6, 5195–5216, 2013

time evolution of $R_{1064}(z)$ on 25 July covering the time interval from 05:00 to 14:15 UT on 30 July 2007, while Fig. 3c illustrates the time evolution of $R_{1064}(z)$ on 30 July covering the time interval from 07:15 to 19:45 UT. The black line in the three figures represents the PBL height as determined through the application of approach(1). In Fig. 3c the black line identifies the PBL height as determined through the application of approach(1) and (2), while the red line identifies the residual layer height in the evening and night portion of the measurement record (determined through approach(1)).

Figure 4 illustrates the evolution of the boundary layer height as obtained from approach(1) and (2) and the radiosonde data for the three case studies on 15, 25 and 30 July 2007. In the figure the continuous lines identify the estimates obtained from approach(1), the yellow stars represent the estimates obtained from the radiosonde potential temperature profiles and the blue squares represent the estimates obtained from approach(2). The figure covers the complete cycle of the PBL evolution including the transitions between day and night and between night and daytime. For all cases the PBL height is found to grow during the day, reaching a maximum value in the early afternoon and then decaying in the late afternoon and evening.

For the purpose of the application of approaches(1) and (2), the signals $P_{\lambda_{EI}}(z)$ and $P_{\lambda_{LoJ}}(z)$ were integrated in time (over a period of 10 min for the former and over a period of 30 min for the latter) and vertically (applying a running average with a vertical window of 150 m over data points separated by 30 m steps). This allowed to reduce signal statistical fluctuations which could affect the applicability of these approaches. Results reveal a very good agreement between the different approaches, with deviations between the different estimates typically not exceeding 200 m.

The approaches described above have been tested on several case studies to verify their applicability in different meteorological conditions, considering convective boundary layers generated in clear-sky conditions and resulting from embedded convection (see Table 1 for a complete list of the selected cases). Figure 5 compares the PBL height estimates obtained with the three different approaches and includes results from all considered case studies (8 in total). Panel a of this figure compares the PBL height

AMTD
6, 5195–5216, 2013

estimates obtained with approach(1) versus the simultaneous radiosonde estimates, while panel b compares the PBL height estimates obtained with approach(2) versus the simultaneous radiosonde estimates. Finally, panel c of this same figure compares the PBL height estimates obtained with approach(1) versus those obtained with approach(2).

Best fit lines are also included in panel a-c based on the application of a least-square fit analysis. The correlation coefficients for these fitting lines are 0.97, 0.92 and 0.90, respectively, while their slopes are 0.97 ± 0.05, 0.94 ± 0.06 and 0.93 ± 0.08, respectively. Values of the correlation coefficients are found to be high for all three comparisons, which testifies the high reliability and reproducibility of the two lidar-based approaches. The mean statistical parameters (number of comparisons, correlation coefficient, standard deviation, absolute and percentage bias and the coefficients of the linear regression) for all case studies are reported in the Table 2. The slope value of 0.97 in Fig. 5a testifies a slight negative bias (3 %) of approach(1) with respect to the traditional approach based on the radiosonde potential temperature profiles, while the slope value of 0.94 in Fig. 5b testifies a slightly larger negative bias (6 %) of approach(2) with respect to the radiosonde estimate. Also approach(1) and (2) are in fairly good agreement, with a relative bias between the two of 7 %. Values of the mean standard deviation (σ) for the PBL height estimates obtained from the compared approaches are found to not exceed 250 m for all comparisons (see Table 2).

Panel d of Fig. 5 illustrates the bias (expressed in %) of approach(1) versus the radiosonde estimates and of approach(2) vs. the radiosonde estimates, while panel e illustrates the bias (expressed in %) of approach(1) vs. approach(2). Most bias values (> 90 %) are found to not exceed 20 %, for all three comparisons, with mean bias values being -3.2, -4.1 and 1.4 %, for approach(1) vs. the radiosonde, for approach(2) vs. radiosonde and for approach(1) vs. approach(2), respectively (see Table 2).

AMTD
6, 5195–5216, 2013

4 Conclusions

The present work compares estimates of the PBL height as obtained from three distinct approaches applied to selected case studies from the COPS experiment. The first approach (called "approach(1)") considers a method based on the identification of minima in the first order derivative of the logarithm of the range-corrected elastic lidar signals. Potential temperature profiles obtained from the radiosondes launched simultaneously to lidar operation are also used to get additional estimates of the boundary layer height, based on the widely used method which considers the transition from a convectively less stable region below to a more stable region above (identified by the level of the maximum vertical gradient). Additional estimates of the boundary layer height and structure are obtained from the identification of minima in the first order derivative of the logarithm of the range-corrected rotational Raman lidar signals (approach(2) or rotational Raman approach), tested for the first time in this paper.

These approaches have been applied to a variety of case studies characterized by different meteorological conditions. A good agreement is found between the three approaches, with the correlation coefficients of the fitting lines representing the comparisons between these approaches being always higher than 0.9. A small negative bias (3 %) is observed between approach 1 and the potential temperature approach, while a slightly larger negative bias (6 %) is found between approach(2) and the potential temperature approach. A fairly good agreement is also found between approach(1) and (2), with a relative bias between the two of 7 %. The good agreement between these different approaches support us on their applicability in different meteorological conditions. In this respect, it is to be pointed out that the dataset collected by BASIL during COPS provides a unique data source for the study of boundary layer structure and evolution.

The use of approach(2) circumvent the problems associated with the application of approach(1) in the presence of strong aerosol gradients observed in the late afternoons and after-sunset, which are representative of a residual aerosol layer aloft the actual

AMTD
6, 5195–5216, 2013

mixed layer, thus allowing unambiguous estimates of the PBL height in any portion of the day.

Acknowledgements. This research effort was partially supported by the European Commission under the European Fleet for Airborne Research program of the 7th Framework Program. We also wish to thank the International Science Steering Committee of the Convective and Orographicallyinduced Precipitation Study for financially supporting this activity.

References

Bhawar, R., Di Girolamo, P., Summa, D., Flamant, C., Althausen, D., Behrendt, A., Kiemle, C., Bosser, P., Cacciani, M., Champollion, C., Di Iorio, T., Engelmann, R., Herold, C., Müller, D., Pal, S., Wirth, M., and Wulfmeyer, V.: The Water Vapour Intercomparison Effort in the Framework of the Convective and Orographically-Induced Precipitation Study: Airborne-to-Ground-based and airborne-to-airborne Lidar Systems, Q. J. Roy. Meteorol. Soc., 137, 325–348, doi:10.1002/qj.697, 2011.

Boers, R., Spinhirne, J. D., and Hart, W. D.: Lidar observations of the fine-scale variability of marine stratocumulus clouds, J. Appl. Meteorol. 27, 797–810, 1988.

Brooks, I. M: Finding boundary layer top: Application of a wavelet covariance transform to lidar backscatter profiles, J. Atmos. Ocean. Technol., 20, 1092–1105, 2003.

Cramer, O. P.: Potential temperature analysis for mountainous terrain, J. Appl. Meteorol., 11, 44–50, 1972

De Wekker, S. F. J., Kossmann, M., and Fielder, F.: Observations of daytime mixed layer heights over mountainous terrain during the TRACT field campaign. Proc. 12th Symp. on Boundary Layers and Turbulence, Vancouver, BC, Canada, Am. Meteorol. Soc., 1, 498–499, 1997.

Di Girolamo, P., Ambrico, P. F., Amodeo, A., Boselli, A., Pappalardo, G., and Spinelli, N.: Aerosol observations by Lidar in the Nocturnal Boundary Layer, Appl. Opt., 38, 4585–4595, doi:10.1364/AO.38.004585, 1999.

Di Girolamo, P., Marchese, R., Whiteman, D. N., and Demoz, B. B.: Rotational Raman Lidar measurements of atmospheric temperature in the UV, Geophys. Res. Lett., 31, L01106, doi:10.1029/2003GL018342, 2004.

Di Girolamo, P., Behrendt, A., and Wulfmeyer, V.: Spaceborne profiling of atmospheric temperature and particle extinction with pure rotational Raman lidar and of relative humidity in

AMTD
6, 5195–5216, 2013

combination with differential absorption lidar: performance simulations, Appl. Opt., 45, 2474–2494, doi:10.1364/AO.45.002474, 2006.
Di Girolamo, P., Summa, D., and Ferretti, R.: Multiparameter Raman Lidar Measurements for the Characterization of a Dry Stratospheric Intrusion Event, J. Atmos. Ocean. Technol., 26, 1742–1762, doi:10.1175/2009JTECHA1253.1, 2009a.
Di Girolamo, P., Summa, D., Lin, R.-F., Maestri, T., Rizzi, R., and Masiello, G.: UV Raman lidar measurements of relative humidity for the characterization of cirrus cloud microphysical properties, Atmos. Chem. Phys., 9, 8799–8811, doi:10.5194/acp-9-8799-2009, 2009b.
Di Girolamo, P., Summa, D., Bhawar, R., Di Iorio, T., Cacciani, M., Veselovskii, I., Dubovik, O., and Kolgotin, A.: Raman lidar observations of a Saharan dust outbreak event: Characterization of the dust optical properties and determination of particle size and microphysical parameters, Atmos. Environ., 50, 66–78, doi:10.1016/j.atmosenv.2011.12.061, 2012a.
Di Girolamo, P., Summa, D., Cacciani, M., Norton, E. G., Peters, G., and Dufournet, Y.: Lidar and radar measurements of the melting layer: observations of dark and bright band phenomena, Atmos. Chem. Phys., 12, 4143–4157, doi:10.5194/acp-12-4143-2012, 2012b.
Flamant C., Pelon, J., Flamant, P. H., and Durand, P.: Lidar determination of the entrainment zone thickness at the top of the unstable marine atmospheric boundary layer, Boundary-Layer Meteorol., 83, 247–284, 1997.
Garratt, J. R.: The Atmospheric Boundary Layer, Cambridge Atmospheric and Space Science Series, Cambridge Univ. Press, 335 pp., 1992
Griaznov, V., Veselovskii, I., Di Girolamo, P., Korenskii, M., and Summa, D.: Spatial distribution of doubly scattered polarized laser radiation in the focal plane of a lidar receiver, Appl. Opt., 46, 6821–6830, 2007.
Haeffelin, M., Angelini, F., Morille, Y., Martucci, G., O'Dowd, C. D., Xueref-Rémy, I., Wastine, B., Frey, S., and Sauvage, L.: Evaluation of mixing depth retrievals from automatic profiling lidars and ceilometers inview of future integrated networks in Europe, Bound.-Layer Meteorol., 143, 49–75, doi:10.1007/s10546-011-9643-z, 2012.
Hastenrath, S.: Climate Dynamics of the Tropics, Kluwer Academic Publishers, Dordrecht, 488 pp., 1991.
Hayden, K. L., Anlauf, K. G., Hoff, R. M., Strapp, J. W., Bottenheim, J. W., Wiebe, H. A., Froude, F. A., Martin, J. B., Steyn, D. G., and McKendry, I. G.: The Vertical Chemical and Meteorological Structure of the Boundary Layer in the Lower Fraser Valley during Pacific "93", J. Atmos. Environ., 31, 2089–2105, 1997.

AMTD
6, 5195–5216, 2013

Hooper, W. P. and Eloranta, E. W.: Lidar measurements of wind in the planetary boundary layer: the method, accuracy and results from joint measurements with radiosonde and Kytoon, J. Clim. Appl. Meteorol., 25, 990–1001, 1986.

Kalthoff, N., Adler, B., Barthlott, C., Corsmeier, U., Mobbs, S., Crewell, S., Trumner, K., Kottmeier, C., Wieser, A., Smith, V., and Di Girolamo, P.: The impact of convergence zones on the initiation of deep convection: A case study from COPS, Atmos. Res., Ed. Elsevier, 93, 680–694, doi:10.1016/j.atmosres.2009.02.010, 2009.

Kottmeier, C., Kalthoff, N., Barthlott, C., Corsmeier, U., Van Baelen, J., Behrendt, A., Behrendt, R., Blyth, A., Coulter, R., Crewell, S., Di Girolamo, P., Dorninger, M., Flamant, C., Foken, T., Hagen, M., Hauck, C., Höller, H., Konow, H., Kunz, M., Mahlke, H., Mobbs, S., Richard, E., Steinacker, R., Weckwerth, T., Wieser, A., and Wulfmeyer, V.: Mechanisms initiating deep convection over complex terrain during COPS, Meteorologische Z., 17, 931–948, 2008.

Mallat, S. G. and Hwang, W. L.: Singularity detection and processing with wavelets, IEEE Trans. Inf. Theory, 38, 617–643, 1992.

Maestri, T., Di Girolamo, P., Summa, D., and Rizzi, R.: Clear and cloudy sky investigations using Raman lidar and airborne interferometric measures from the European AQUA Thermodynamic Experiment, Atmos. Res., 97, 157–169, doi:10.1016/j.atmosres.2010.03.020, 2010.

Martucci, G., Matthey, R., Mitev, V., and Richner, H.: Comparison between backscatter lidar and radiosonde measurements of the diurnal and nocturnal stratification in the lower troposphere, J. Atmos. Ocean. Technol., 24, 1231–1244, 2007.

Martucci, G., Matthey, R. , Mitev, V., and Richner, H.: Frequency of boundary-layer-top fluctuations in convective and stable conditions using laser remote sensing, Bound.-Layer Meteorol., 135, 313–331, 2010.

Melfi, S. H., Spinhirne, J. D., Chou, S. H., and Palm, S. P.: Lidar observation of the vertically organized convection in the planetary boundary layer over the ocean, J. Clim. Appl. Meteorol., 24, 806–821, 1985.

Morille, Y., Haeffelin, M., Drobinski, P., and Pelon, J.: STRAT: An Automated Algorithm to Retrieve the Vertical Structure of the Atmosphere from Single-Channel Lidar Data, J. Atmos. Ocean. Technol., 24, 761–775, 2007.

Oke, T. R.: Boundary Layer Climates, 2nd Edn., 435 pp., Halsted Press, New York, 1988.

Seibert, P., Beyrich, F., Gryning, S. E., Joffre, S., Rasmussen, A., and Tercier, P.: Review and Intercomparison of Operational Methods for the Determination of the Mixing Height, Atmos. Environ., 34, 1001–1020, 2000.

AMTD
6, 5195–5216, 2013

Sicard, M., Pérez, C., Rocadembosch, F., Baldasano, J. M., and Garcìa-Vizcaino, D.: Mixed layer determination in the Barcelona coastal area from regular lidar measurements: methods, results and limitations, Bound.-Layer Meteorol., 119, 135–157, 2006.

Stull, R. B.: An Introduction to Boundary Layer Meteorology, Dordrecht, Kluwer, 666 pp., 1998

Sorbjan, Z.: Structure of the Atmospheric Boundary Layer, Prentice Hall, Englewood Cliffs, N.J., 317 pp., 1989

Van Pul, W. A. J., Holtslag, A. A. M., and Swart, D. P. J.: A comparison of ABL heights inferred routinely from lidar and radiosondes at noontime, Bound.-Layer Meteorol., 68, 173–191, 1994.

Wulfmeyer, V., Behrendt, A., Bauer, H. S., Kottmeier, C., Corsmeier, U., Blyth, A., Craig, G., Schumann, U., Hagen, M., Crewell, S., Di Girolamo, P., Flamant, C., Miller, M., Montani, A., Mobbs, S., Richard, E., Rotach, M. W., Arpagaus, M., Russchenberg, H., Schlüssel, P., König, M., Gärtner, V., Steinacker, R., Dorninger, M., Turner, D. D., Weckwerth, T., Hense, A., and Simmer, C.: The Convective and Orographically-induced Precipitation Study: A Research and Development Project of the World Weather Research Program for Improving Quantitative Precipitation Forecasting in Low-mountain Regions, B. Am. Meteorol. Soc., 89, 1477–1486, doi:10.1175/2008BAMS2367.1, 2008.

Wulfmeyer, V., Behrendt, A., Kottmeier, C., Corsmeier, U., Barthlott, C., Craig, G. C., Hagen, M., Althausen, D., Aoshima, F., Arpagaus, M., Bauer, H. S., Bennett, L., Blyth, A., Brandau, C., Champollion, C., Crewell, S., Dick, G., Di Girolamo, P., Dorninger, M., Dufournet, Y., Eigenmann, R., Engelmann, R., Flamant, C., Foken, T., Gorgas, T., Grzeschik, M., Handwerker, J., Hauck, C., Höller, H., Junkermann, W., Kalthoff, N., Kiemle, C., Klink, S., König, M., Krauss, L., Long, C. N., Madonna, F., Mobbs, S., Neininger, B., Pal, S., Peters, G., Pigeon, G., Richard, E., Rotach, M. W., Russchenberg, H., Schwitalla, T., Smith, V., Steinacker, R., Trentmann, J., Turner, D. D., van Baelen, J., Vogt, S., Volkert, H., Weckwerth, T., Wernli, H., Wieser, A., Wirth, M.: The Convective and Orographically Induced Precipitation Study (COPS): The Scientific Strategy, the Field Phase, and Research Highlights, Q. J. Royal Meteorol. Soc., 137, 3–30, doi:10.1002/qj.752, 2011.

AMTD
6, 5195–5216, 2013

Table 1. List of the considered case studies with a description of the weather condition.

Date(s)	IOP	Weather condition
19 June 2007	IOP4	Shallow Convection. Shower during the day
15 July 2007	IOP8	Shallow Convection. No precipitation
19 July 2007	IOP9	MCS Moving over COPS region followed by partially convective precipitation
25 July 2007	IOP11	Cumulus convection mostly over the mountains
30 July 2007	IOP12	Cumulus convection
1 August 2007	IOP13	Cloud-free weather under a hight-pressure ridge; Sharan dust over COPS domain
6 August 2007	IOP14	Isolated storm over the entire COPS domain followed by a large area of elevated precipitation
12 August 2007	IOP15	Storm over the eastern Black Forest and Swabian Jura

AMTD
6, 5195–5216, 2013

Table 2. Mean statistical parameters for the comparisons involving the different methods. The different columns list the approach, the correlation coefficient, R, the standard deviation, σ, the number of comparisons, the absolute and percentage mean bias, the coefficients of the linear regression. The percentage mean bias between two methods was calculated as the ratio (expressed in percentage) of deviation between the two over the mean value of the two.

Approach	R	σ (m)	# comparisons	Mean bias (m)	Mean bias (%)	Linear Regression: $Y = a^*X + b$
Approach(1) vs. RS	0.97	185	30	150	−3.2	$a = 0.97$; $b = 21.6$
Approach(2) vs. RS	0.92	248	30	198	−4.1	$a = 0.94$; $b = 167.5$
Approach(1) vs. approach(2)	0.90	213	115	160	1.4	$a = 0.93$; $b = 81.0$

AMTD
6, 5195–5216, 2013

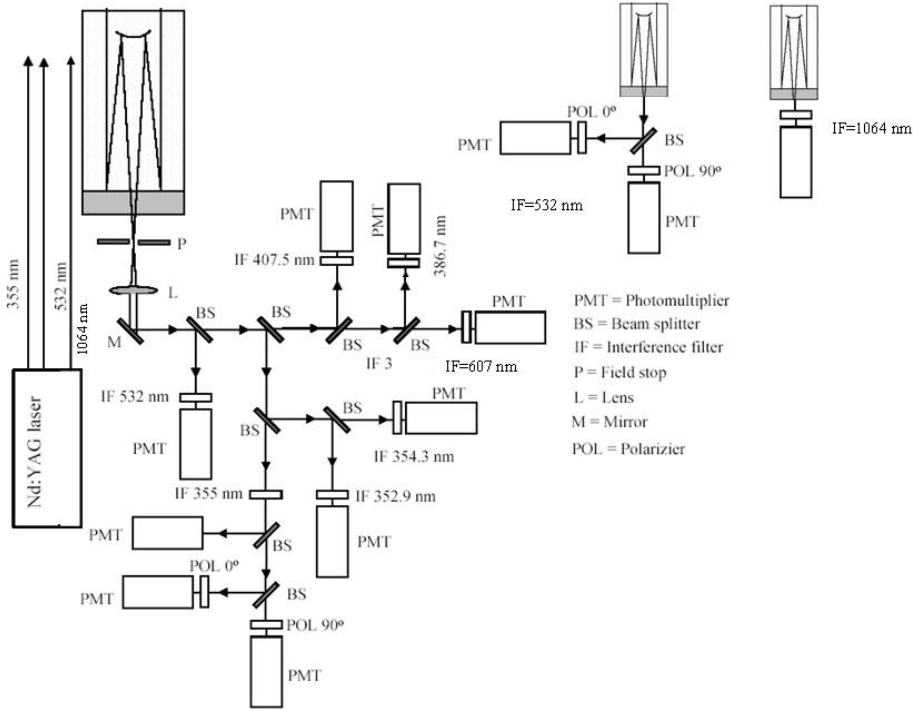

Fig. 1. Block diagram of the setup of the Raman lidar system BASIL during COPS.

AMTD
6, 5195–5216, 2013

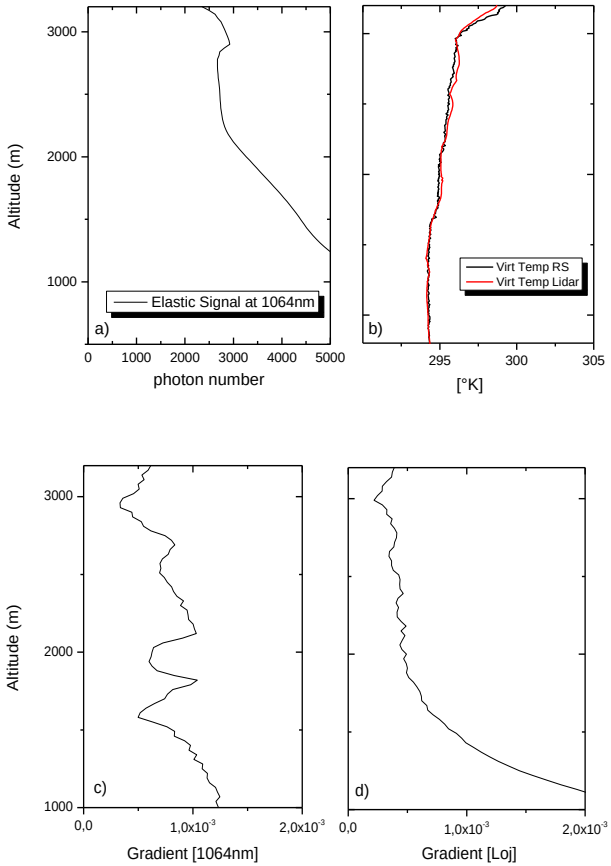

Fig. 2. (a) 10-min average profile of $P_{\lambda_{El}}(z)$ centered at 17:04 UTC on 30 July 2007 as measured by BASIL. **(b)** Vertical profiles of virtual potential temperature as measured by BASIL and the radiosonde launched at 17:04 UTC. **(c)** Vertical gradient of $P_{\lambda_{El}}(z)$ for the same 10 min time interval considered in **(a)**. **(d)**: vertical gradient of $P_{\lambda_{LoJ}}(z)$ for the same 10 min time interval considered in **(a)**.

AMTD
6, 5195–5216, 2013

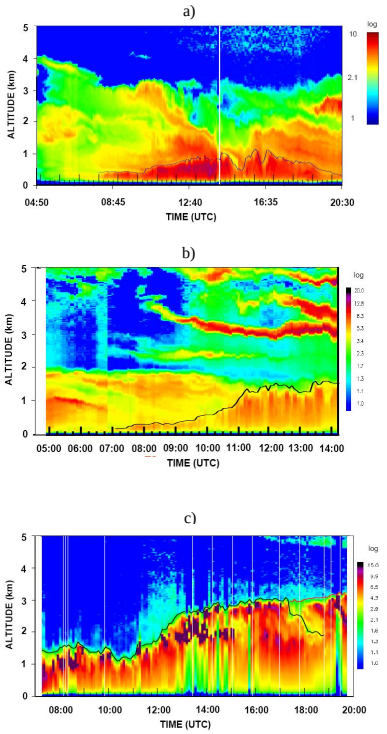

Fig. 3. Time evolution of the particle backscattering ratio at 1064 nm as measured by BASIL from 04:50 to 20:30 UT on 15 July 2007 **(a)**; from 05:00 to 14:15 UT on 25 July 2007 **(b)** and from 07:15 to 19:45 UT on 30 July 2007 **(c)**. In panel a and b the black line identifies the PBL height as determined through the application of approach(1); in **(c)** the black line identifies the PBL height as determined through the application of approach(1) and (2), while the red line identifies the residual layer height in the evening and night portion of the measurement session as determined through the application of approach(1).

AMTD
6, 5195–5216, 2013

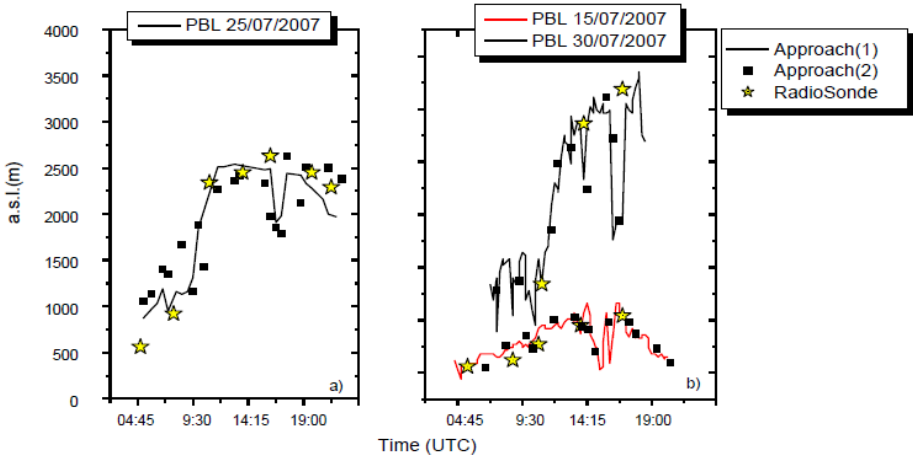

Fig. 4. Evolution of the PBL height for 15, 25 and 30 July 2007. The continuous lines identify the PBL height estimates obtained from approach(1), the yellow stars represent estimates obtained from the potential temperature profiles as measured by the radiosondes and the blue squares represent the estimates obtained from approach(2).

AMTD
6, 5195–5216, 2013

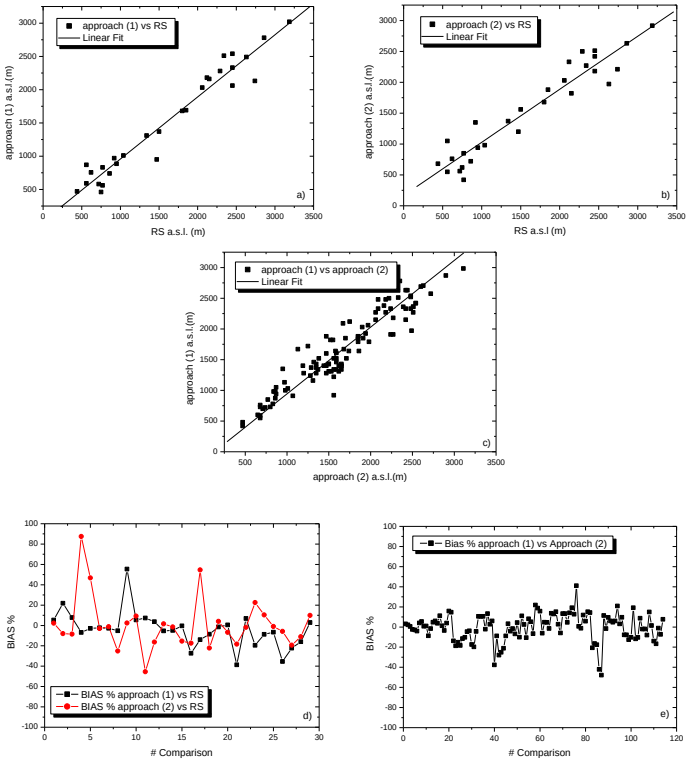

Fig. 5. Comparison of PBL height estimates obtained with different approaches: **(a)** approach(1) versus simultaneous radiosonde estimates; **(b)** approach(2) versus simultaneous radiosonde estimates; **(c)** approach(1) versus approach 2; **(d)** bias (expressed in %) of approach1 vs radiosonde estimates (squares) and of approach(2) vs radisonde estimates (circles). **(e)** bias (expressed in %) of approach(1) vs approach(2). In panel **(a–c)** best fit lines are also included.

AMTD
6, 5195–5216, 2013